Kinetics of Tetracycline Degradation in Visible-Light-Driven Photocatalysis using g-C_3N_4 and Effects of Low-Molecular-Weight Organic Acids

P.A.S.A. Pannala[1,2] and Jenyuk Lohwacharin[3*]

[1]International Program in Hazardous Substance and Environmental Management (IP-HSM), College of Interdisciplinary and Integrative Studies, Chulalongkorn University, Bangkok 10330, Thailand
[2]Center of Excellence on Hazardous Substance Management (HSM), Chulalongkorn University, Bangkok 10330, Thailand
[3]Department of Environmental and Sustainable Engineering, Chulalongkorn University, Bangkok 10330, Thailand
**Corresponding Author E-mail: jenyuk.l@Chula.at.th*

ABSTRACT

Tetracycline (TC) is a broadly detected antibiotic residue in surface water and wastewater. Visible-light photocatalytic removal of TC is affected by the presence of co-occurring low-molecular-weight organic acids (LMWOAs). Although removal efficiency is usually used to measure the effectiveness of these systems, reaction kinetics and practical energy cost are important for the process to be scaled up from the laboratory and designed for the engineering scale and are measured for the first time for this system. This study uses pseudo-first order (PFO), pseudo-second order (PSO) and Langmuir–Hinshelwood (L–H) kinetic models to fit a photodegradation dataset involving salicylic acid (SA) and malic acid (MA) as modelled co-contaminants and assesses process performance through the Electrical Energy per Order (EEO) metric under g-C_3N_4/LMWOA. The synthesized g-C_3N_4 photocatalyst was physicochemically characterized to ensure its suitability to operate under visible-light. The PFO model was found to fit best and most physically consistently under all conditions (R^2 = 0.969–0.993) and a single-run L–H analysis confirmed that the rate and adsorption parameters of the L–H model are not simultaneously separable when the fractional surface coverage remains low (i.e., $K \cdot C \ll 1$, the regime in which the Langmuir–Hinshelwood rate law mathematically reduces to pseudo-first-order kinetics), further supporting PFO as the appropriate apparent kinetic description of the system under the conditions tested. The presence of SA resulted in a 4.4–7.4-fold increase in the EEO and a 80.5–89.0% decrease in the apparent rate constant, *k1*, while the EEO was found to increase by 1.09–1.35-fold and the k_1 was decreased by 14.4–30.5% in the presence of MA. The results will give practical, engineering-oriented benchmarks for scale-up of g-C_3N_4 based photocatalytic system for the treatment of water contaminated with antibiotics under varying conditions of real-world water-matrix.

Keywords: Tetracycline/ Photocatalytic kinetics/ Low-molecular-weight organic acids

1. INTRODUCTION

Antibiotic residues are increasingly recognized as contaminants of emerging concern in aquatic environments globally. Tetracycline (TC) is one of the most widely used broad-spectrum antibiotics in human medicine, animal husbandry and aquaculture, and because it is not fully metabolized and the disposal is not appropriate, it is often found in surface water, groundwater and municipal and agricultural wastewater [1]. TC persistence in aquatic environments is also a concern due to the potential for the emergence of antibiotic-resistant bacteria and long-term ecotoxicological impacts and is anticipated to increase as climate change alters runoff patterns, water availability and contaminant loading, driving a need for climate-resilient, low carbon treatment options [2].

Semiconductor photocatalysis has developed as a promising, low carbon advanced oxidation process (AOP) for antibiotic removal, with particular interest in graphitic carbon nitride (g-C_3N_4) as a promising metal-free photocatalyst that is visible-light responsive with an appropriate band gap, it has a heptazine-type layered structure, is chemically stable and is easy to prepare and scale up [3, 4]. Moreover, g-C_3N_4 has visible light activity and is suitable for solar and low energy LED irradiation, making it an ideal material for decentralized, climate-proof water treatment in resource-limited locations. However, in real wastewater and agricultural run-off, TC is not always the only contaminant present; often low-molecular-weight organic acids (LMWOAs) like malic acid and salicylic acid,

common constituents of pharmaceutical, agricultural, and food-processing effluents, can affect the photocatalytic action through various mechanisms, such as light shielding and surface complexation, as well as hole scavenging [5].

Salicylic acid (SA) and malic acid (MA) were chosen as model LMWOAs as each of them is a realistic co-occurrence pathway with TC and the reported environmental and wastewater concentrations fall in the range of 0.5 to 5 mM, which was tested in this study. SA is itself a pharmaceutical (the main metabolite of aspirin, active ingredient in dermatological products) and is one of the most frequently detected acidic pharmaceuticals in paired surface-water/wastewater surveys alongside antibiotics and other pharmaceuticals, with a 100% detection rate in a recent 97-compound screening study [6]. Surface-water concentrations of SA are generally in the nanogram per liter range, while concentrations up to the low microgram per liter range have been reported in sewage after surveys of sewage sources from ozonation plants [7]. In fact, the concentration range used in the present study fully overlaps with the concentrations reported for wastewater-treatment-plant (WWTP) influents [8] to be between 3–900 mgL^{-1} (≈ 0.02–6.5 mM). The concentration of MA in fruit-processing wastewater and in orchard drainage containing residues of such fruit-processing should be anticipated to be at or above the tested range because MA is a dominant organic acid of apple and other fruit juices present at 3–8 gL^{-1} (≈ 22–60 mM) and varying by several g L^{-1} with changes in fruit storage and processing conditions [9]. In addition, there is a second, independent pathway for agricultural runoff and manure drainage to reach surface levels of MA-type acids within the range of concentrations tested, with total LMWOA concentrations of 10–25 mM associated with mobilization of soil nutrients [10]. Livestock wastewater and manure are both a significant source of tetracycline-class antibiotics and a source of elevated levels of organic-acid loading; and exposure to these organic acids has been shown to lead to increased VOCs in the treated manure during anaerobic digestion when the manure is contaminated with TC [11], making it a realistic exposure condition for a field-deployed g-C_3N_4 photocatalytic system. The concentration range tested in this study is 0.5–5 mM, which is a realistic exposure scenario.

The g-C_3N_4 photocatalyst was synthesized and physicochemically characterized and evaluated its performance in the degradation of TC under visible light in the presence of SA and MA. However, removal efficiency is not enough to define practical process design since the kinetic parameters of the reaction, and the energy requirement of the process are the ones that define its technical and economic feasibility when applied to real water treatment. A percentage removal efficiency does not necessarily determine how long a reactor needs to run to achieve a specified discharge standard, how that operating time changes from one influent LMWOA profile to another, or how much energy a full-scale system requires for each scenario; all of these quantities depend on the rate constants and Electrical Energy per Order (EEO) and not on the removal efficiency alone. This quantitative, process-oriented, modelling dimension of g-C_3N_4/TC/LMWOA has not been reported so far.

The study aims at (i) summarizing the key physicochemical properties of the synthesized g-C_3N_4 photocatalyst that account for its photocatalytic behavior; (ii) fitting the time courses of the TC removal to the pseudo-first-order, pseudo-second-order, and Langmuir–Hinshelwood kinetic models to obtain apparent rate constants, and critically testing which model is not just the best statistical fit, but the physically correct one for the system; (iii) evaluating the EEO, a standard engineering benchmark used for AOP, and converting the obtained apparent rate constants to the corresponding energy-cost benchmark that is commonly reported in the AOP literature; and (iv) comparing the observed kinetic response with simplified structural descriptors of the tested organic acids. The goal is to develop laboratory-based mechanistic insights into engineering relevant, decision-ready kinetic and energy benchmarks that enable the practical, real-world application of g-C_3N_4-based photocatalysis for antibiotic contaminated water treatment.

2. METHODOLOGY

2.1 Photocatalyst Synthesis and Characterization

In this work, the g-C_3N_4 photocatalyst was synthesized by thermal polymerization of urea [12],

and characterized by X-ray diffraction (XRD), Fourier-transform infrared spectroscopy (FTIR), and laser diffraction particle-size analysis and nitrogen (N_2) physisorption (BET/BJH). Table 1 shows the main characterization results, and they will be used directly in the interpretation of the kinetic and energy-efficiency results in Sections 3.2–3.4; therefore, they are presented briefly.

2.2 Photocatalytic Experiments

The batch photocatalytic experiments were conducted in 300 mL of aqueous TC solution laden with the selected LMWOAs, either SA or MA, at the initial concentrations of 0.5, 1, 2 and 5 mM. The initial TC concentration was 20 mg L^{-1}, and the g-C3N4 photocatalyst dosage was 0.1 g (0.333 g L^{-1}) in all experiments. Irradiation was provided by a 300 W visible-light xenon lamp equipped with a 420 nm cut-off filter, with a measured light intensity of 10.81 mW cm^{-2} at the reactor surface. Residual TC concentration was determined at 357 nm using a UV–Vis spectrophotometer (Model UH5300, Hitachi). All experiments were performed in duplicate, and the mean ± standard deviation is reported in Table 2 where applicable.

Dark-adsorption was first performed for 30 minutes to achieve the adsorption–desorption equilibrium before irradiation. Aliquots (3 mL) were taken at 0, 15 and 30 minutes of the dark period and every 10 minutes from then on (up to 150 min) after visible-light irradiation and the remaining TC concentration measured using a UV–Vis calibration graph. The kinetic and energy analysis in this paper is based on these TC concentration–time datasets obtained from these experiments where the concentration at the beginning of the irradiation (after the dark equilibration) is taken as C_0 for kinetic modelling as is usual for heterogeneous photocatalytic systems.

2.3 Kinetic Modelling

Three kinetic models commonly applied to heterogeneous photocatalytic degradation were fitted to the TC concentration–time data for each condition:

Pseudo-first-order (PFO): $ln(C_t/C_o) = - k_1 t$ [13] (1)
Pseudo-second-order (PSO): $1/C_t - 1/C_0 = k_2 t$ (2)
Langmuir–Hinshelwood (L–H), integrated batch form: $k_r t = (C_0 - C_t) + (1/K)\, ln(C_0/C_t)$ [14] (3)

Where C_0 and C_t are the TC concentrations at time 0 and time t, respectively; k_1 and k_2 are the apparent PFO and PSO rate constants; and k_r and K are the L–H surface reaction rate constant and adsorption equilibrium constant, respectively. The PFO and PSO models were fitted by standard linear regression forced through the origin. The L–H model is particularly useful because the k_r and K parameters can be resolved independently by running the series of reactions at different initial TC concentrations as was done in the traditional approach; however, the present dataset included a variable concentration of LMWOA at a fixed initial TC concentration, and therefore the k_r and K parameters were estimated directly from the full concentration–time profile of each individual run, following the single-run integral-method approach recently validated for heterogeneous photocatalytic systems [14]. An unconstrained least-squares fit and a physically constrained fit (k_r, $K \geq 0$) were used for all conditions, and the parameters and fit quality, e.g., the coefficient of determination R^2, were evaluated with regard to the practical identifiability of the L–H model for this system, as described in Section 3.3. The best fit model for each condition was chosen as per R^2 and physically plausible parameters for each model.

2.4 Electrical Energy per Order (E_{EO})

The *EEO* (Electrical Energy per Order) figure of merit, recommended by IUPAC for benchmarking the energy efficiency of advanced oxidation processes [15], was used to evaluate the energy demand of the photocatalytic process under each condition:

$$E_{EO}\ (\text{kWh m}^{-3}\ \text{order}^{-1}) = (P \times t \times 1000) / (V \times 60 \times \log(C_0/C_t)\ \ [15] \quad (4)$$

Where P is rated lamp power (0.3 kW), t is the irradiation time (150 min), and V is the volume of the solution to be treated (0.3 L). EEO is the electrical energy needed to decrease the pollutant concentration by one order of magnitude in 1 m^3 of contaminated wastewater; the smaller the EEO, the more energy efficient the process is. The absolute value obtained here represents the small-volume, high-irradiance, bench-scale reactor for this study, and a relative comparison of the reactors within the EEO study (compared to the absolute value) is the engineering scale-up benchmark.

2.5 Structure–Kinetics Comparison

To determine whether the observed kinetic response is related to the structure of the organic acids, apparent rate constants (k_1) from the lowest common dose (0.5 mM) were compared with two commonly used structural features of the acid, the number of carboxyl (–COOH) groups and the first acid dissociation constant (pKa_1) for each acid.

3. RESULTS AND DISCUSSION

3.1 Photocatalyst Characterization

The key physicochemical properties of the synthesized g-C_3N_4 photocatalyst are summarized in Table 1. The XRD pattern exhibited two main reflections at 2θ = 12.8° and 27.6° indicative of the (100) and (002) planes of g-C_3N_4 and in good agreement with the two peaks reported for thermally polymerized g-C_3N_4 [3]. The characteristic C–N/C=N heptazine ring vibrations (1200 – 1650 cm^{-1}) and the breathing mode for the tri-s-triazine (805.5 cm^{-1}) were confirmed by FTIR. The indirect band gap obtained from UV–Vis DRS was 2.85 eV, in the range reported by Briševac et al., 2025 for bulk g-C_3N_4 obtained by thermal polymerization [16], and in line with the irradiation by visible light (>420 nm) applied in this study. The BET analysis shows a BET surface area of 97.78 $m^2\ g^{-1}$ and a total pore volume of 0.178 $cm^3\ g^{-1}$.

Table 1. Summary of g-C_3N_4 photocatalyst characterization results.

Technique	Key result
XRD	(100) and (002) reflections at 2θ = 12.8° and 27.6°; interlayer distance ≈ 0.32 nm
FTIR	N–H/O–H (3000–3400 cm^{-1}); C–N/C=N heptazine ring (1200–1650 cm^{-1}); tri-s-triazine breathing (805.5 cm^{-1})
UV–Vis DRS	Absorption edge ≈ 431 nm; indirect band gap = 2.85 eV
Particle size (laser diffraction)	D(v,0.5) = 34.06 μm; D(v,0.1)/D(v,0.9) = 7.41/88.33 μm; D[4,3] = 43.04 μm
N_2 physisorption (BET/BJH)	Type IV isotherm, H3 hysteresis (mesoporous); S_{eet} = 97.78 $m^2\ g^{-1}$; pore volume = 0.178 $cm^3\ g^{-1}$; pores mainly 2–30 nm

3.2 Kinetics of TC Photodegradation

The parameters of PFO and PSO kinetic models obtained by model fitting are summarized in Table 2 for TC degradation without and with SA and MA. The low, environmentally relevant TC concentrations used in the study and previous literature reporting PFO kinetics dominating dilute systems with heterogeneous catalysts [13] , are consistent with the better fit of the PFO model for every condition tested (R^2 = 0.969–0.993, compared to 0.961–0.977 for PSO).

Table 2. Pseudo-first order (PFO) and pseudo-second order (PSO) kinetic parameters for the TC photodegradation in the presence of g-C_3N_4 under various LMWOA conditions.

Condition	k_1 (min^{-1})	R^2 (PFO)	k_2 ($mg^{-1}\cdot L\cdot min^{-1}$)	R^2 (PSO)	$t_{1/2}$ (min)
g-C_3N_4 only (control)	0.0118 ± 0.00013	0.989	0.0409 ± 0.00134	0.9716	58.7 ± 0.7
+ SA 0.5 mM	0.0023 ± 0.00002	0.985	0.0046 ± 0.00010	0.9761	301.4 ± 2.8
+ SA 1 mM	0.0022 ± 0.00004	0.9857	0.0048 ± 0.00002	0.9771	315.1 ± 5.1
+ SA 2 mM	0.0017 ± 0.00001	0.977	0.0035 ± 0.00004	0.9681	407.7 ± 3.3
+ SA 5 mM	0.0013 ± 0.00003	0.9698	0.0025 ± 0.00006	0.9628	533.2 ± 11.4
+ MA 0.5 mM	0.0101 ± 0.00035	0.9921	0.0384 ± 0.00375	0.9613	68.6 ± 2.4
+ MA 1 mM	0.0097 ± 0.00045	0.9916	0.034 ± 0.00353	0.9619	71.5 ± 3.3
+ MA 2 mM	0.0092 ± 0.00071	0.9931	0.0324 ± 0.00693	0.9612	75.3 ± 5.8
+ MA 5 mM	0.0082 ± 0.00001	0.9928	0.0265 ± 0.00255	0.9717	84.5 ± 0.1

Despite being classified as carboxylic acids, the two organic acids showed very different kinetic responses. Within the range of 0.5–5 mM, the k_1 of the system laden with SA was found to be 80.5–89.0% lower than the control (k_1 = 0.0118 min^{-1}), which resulted in an increase in the half-life ($t_{1/2}$) from 58.7 to 301–533 minutes. MA, on the other hand, reduced the k_1 by ca. 14.4–30.5%, and the $t_{1/2}$ was only extended up to 68.6–84.5 minutes, which is just slightly longer than the control, and hence very little difference in the treatment time. The large difference in kinetic separation between the two LMWOAs signifies that SA is much more reactive with the photocatalytic system than MA, emphasizing roles of carboxylic molecular structure in competing with TC upon photocatalytic degradation.

3.3 Langmuir–Hinshelwood Analysis

Table 3 shows data from a single-run fit of the integrated single-run L–H equation (Equation (3)) using the whole time-dependent decay data for each condition, both with an unconstrained least-squares regression and a physically constrained regression that assumes k_r, $K \geq 0$.

Table 3. Langmuir–Hinshelwood parameters for TC photodegradation over g-C3N4 under different LMWOA conditions.

Condition	k_r (unc.)	K (unc.)	R^2 (unc.)	k_r (cons.)	K (cons.)	R^2 (cons.)
Control	−0.125	−0.053	0.960	0.138	→ 0 (bound)	0.161
+ SA 0.5 mM	−0.071	−0.026	0.998	0.041	→ 0 (bound)	0.980
+ SA 1 mM	−0.027	−0.044	0.994	0.037	→ 0 (bound)	0.977
+ SA 2 mM	0.020	−0.178	0.996	0.033	→ 0 (bound)	0.996
+ SA 5 mM	0.012	−0.120	0.999	0.026	→ 0 (bound)	0.997
+ MA 0.5 mM	−0.157	−0.048	0.980	0.117	→ 0 (bound)	0.333
+ MA 1 mM	−0.181	−0.040	0.986	0.132	→ 0 (bound)	0.430
+ MA 2 mM	−0.172	−0.041	0.994	0.119	→ 0 (bound)	0.418
+ MA 5 mM	−0.129	−0.044	0.992	0.113	→ 0 (bound)	0.488

This analysis leads to two conclusions. In the first place, for most of the conditions, the unconstrained L–H regression yielded negative values of k_r and K even though the nominal R^2 was high, which is a physically meaningless result as both parameters are supposed to be non-negative. Second, when both regression is forced to physically valid values (k_r, $K \geq 0$) they are driven to the lower boundary (in other words, $K \rightarrow 0$) on each of the conditions, and the fit quality is poor for the control and all MA conditions (R^2 = 0.161 to 0.488) but acceptable for the SA series (R^2 = 0.977–0.997) with K still undetermined at the lower boundary. This signature is what one would expect if the parameters were not identifiable, which is a direct consequence of the L–H rate law itself. Starting from the general form as shown in equation (5) [13],

$$-dC/dt = k_r KC / (1 + KC) \quad (5)$$

When one batch run is still in the low-surface-coverage, dilute regime ($K \cdot C \ll 1$, as was found before in excellent PFO R^2, Section 3.2), the denominator becomes $1 + KC \approx 1$, and the rate law reduce to equation (6):

$$-dC/dt \approx k_r KC = k_1 C \text{ (with } k_1 \equiv k_r K) \quad (6)$$

Integrating from C_0 to C_t recovers exactly the PFO equation used in Table 2 (Equation (1)): $\ln(C_0/C_t) = -k_1 t$

However, it is not possible to determine both the values of k_r and K from a single dilute-regime run of the experiment, the only thing that can be determined is the value of $k_r K$; any pair of values that satisfy $k_r K = k_1$ will fit the same data equally well. This is just the situation where a one-run L–H fit is known to be ill-posed [14]. The collapse in fit quality is most pronounced in the runs with the lowest degree of curvature away from simple exponential decay (the control and MA runs) and weakest (but still boundary-pinned) in the more strongly inhibited SA runs. Rather than omitting the L–H model, this analysis is reported in full because the identifiability failure is itself an informative, quantitative result: it shows that PFO is not merely the best-fitting model among those tested, but the most defensible apparent kinetic description for this g-C_3N_4/TC system at the concentrations tested. Resolving k_r and K independently would require a dedicated multi-concentration isotherm series, consistent with the traditional L–H requirement [13], which is beyond the scope of the present kinetic dataset.

This pattern is evident directly in Figure 1; the PFO and PSO bars are consistently high (R^2 > 0.96) over all nine conditions; the constrained L–H bars show a close relationship with the PFO and PSO bars only for the SA series, but they drop precipitously for the control and MA conditions, reaching 0.161 at the lowest point.

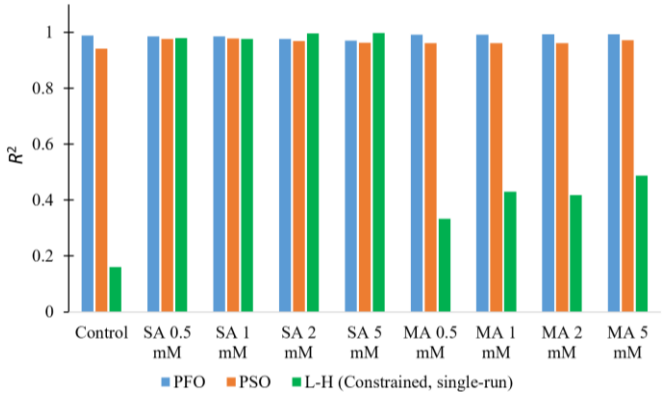

Figure 1. Coefficient of determination (R^2) for PFO, PSO, and physically constrained single-run L–H fits, by condition.

3.4 Energy-Efficiency Assessment (E_{EO})

The resulting EEO values for each condition are shown in Table 4 during treatment time of 150 min with the fixed reactor parameters of P = 0.3 kW and V = 0.3 L.

Table 4. Electrical Energy per Order (E_{eo}) for TC photodegradation over g-C_3N_4 under different LMWOA conditions (P = 0.3 kW, V = 0.3 L, t = 150 min).

Condition	P (kW)	V (L)	log(C_0/C_t)	E_{EO} (kWh m^{-3} order^{-1})
g-C_3N_4 only (control)	0.3	0.3	0.837	2,986
+ SA 0.5 mM	0.3	0.3	0.189	13,204
+ SA 1 mM	0.3	0.3	0.181	13,804
+ SA 2 mM	0.3	0.3	0.149	16,793
+ SA 5 mM	0.3	0.3	0.113	22,179
+ MA 0.5 mM	0.3	0.3	0.772	3,241
+ MA 1 mM	0.3	0.3	0.749	3,339
+ MA 2 mM	0.3	0.3	0.723	3,458
+ MA 5 mM	0.3	0.3	0.623	4,016

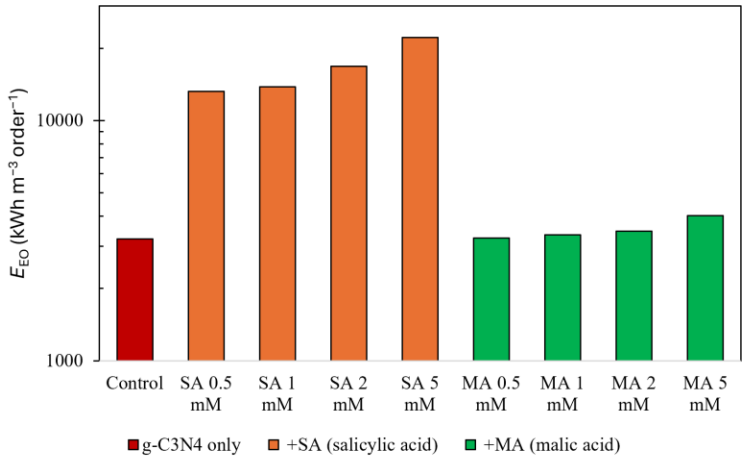

Figure 2. Electrical Energy per Order (E_{EO}) for TC photodegradation over g-C_3N_4 as a function of LMWOA identity and concentration (log scale).

The absolute EEO values obtained (2,986–22,179 kWh m^{-3}order^{-1}; Figure 2) are typical of the small-volume (0.3 L), high-irradiance (0.3 kW) bench-scale reactor used in this study and are comparable or higher than those reported by other lab-scale AOP reactors with similar power-to-volume ratio, while pilot and full-scale reactors with larger treated volumes typically report values of 1–2 orders of magnitude lower. High EEO values have also been reported for laboratory-scale photocatalytic systems using high-power xenon lamps. For example, Kokate et al. (2022) reported an EEO of 2,702 kWh m^{-3} order^{-1} for peroxymonosulfate-activated Acid Orange 7 degradation by g-C3N4 under xenon irradiation [17] . In the same study, switching from the xenon lamp to a low-power (1.54 W) 400 nm LED reduced the EEO by approximately 110-fold to 24.51 kWh m^{-3} order^{-1}. Similarly, Ma et al. (2024) reported EEO values of 4,021–7,462 kWh m^{-3}order^{-1} for tetracycline degradation using a TiO2@g-C3N4 photocatalyst under xenon irradiation [18]. These studies demonstrate that high EEO values can occur in small-scale photocatalytic systems using high-power xenon lamps and that lamp power is an

important factor affecting EEO. Therefore, replacing the 300 W lamp used here with a lower-power, spectrally matched LED source could be a natural next step for reducing the energy cost of this system at pilot scale, without necessarily changing the photocatalyst or the chemistry. The relative trend across conditions is therefore the primary engineering signal of interest here.

The effect of co-occurring water-matrix constituents on the energy required to achieve EEO is well documented for UV- and photocatalysis-based AOPs applied to pharmaceuticals: an EEO of more than 5.5 fold higher was reported when synthetic surface water was used instead of ultrapure water in the direct TiO_2 photocatalysis study [19], while a systematic review across several UV-AOP technologies treating pharmaceuticals revealed that co-occurring water-matrix constituents consistently increased the electrical energy demand for the degradation of pharmaceuticals [20]. A comparable magnitude has also been reported for the lab-scale photocatalytic degradation of the antibiotic metronidazole with TiO_2, where a bench-scale reactor with a power-to-volume ratio of 0.125 kW L^{-1} (125 W lamp, 1 L working volume) gave EEO values of 93.6–666.7 kWh m^{-3} $order^{-1}$ using the identical formula [18]; the present reactor's higher power-to-volume ratio (0.3 kW / 0.3 L = 1.0 kW L^{-1}) is consistent with its correspondingly higher EEO values here. The enhancement in EEO was 4.4 - 7.4 times those of the control, suggesting that, at bench scale, a reactor treating SA-containing water would need to expend roughly 4–7 times more electrical energy to obtain the same order-of-magnitude TC reduction under the tested conditions; this extrapolation should be treated as indicative rather than predictive, since reactor configuration, irradiation efficiency, and other scale-up factors may substantially alter the actual energy demand of a full-scale system. The relatively small energy penalty for MA was a mere 1.09–1.35-fold increase in EEO. At 0.5 mM, the EEO was lowest (3,241 kWh m^{-3} $order^{-1}$) and this condition was identified as the most energy-efficient, "optimal", LMWOA condition tested, with only 8.5% increase in EEO over the control.

3.5 Structure–Kinetics Relationship

Table 5 compares the apparent rate constant at the lowest common dose (0.5 mM) with two simple structural descriptors of the acids tested.

Table 5. Relationship between organic-acid structure and apparent pseudo-first-order rate constant at 0.5 mM**.**

Organic acid	No. of –COOH groups	pKa_1	k_1 at 0.5 mM (min^{-1})	k_1 relative to control
Salicylic acid (SA)	1	2.97	0.0023	−80.5%
Malic acid (MA)	2	3.40	0.0101	−14.4%

The large difference between the two inhibitions for SA and MA cannot be attributed to the number of carboxyl groups or their acidity alone. MA has two carboxyl groups, but despite this it caused much less inhibition of TC degradation, compared to SA. This means that the overall molecular structure and the interaction between LMWOA and the g-CN surface can also affect the photocatalytic kinetics observed. Carboxylic acids can coordinate to the semiconductor and oxide surface in various ways, including monodentate and bidentate binding, and the strength of these interactions is related to the molecular structure [21]. The existence of both a carboxyl group and a phenolic group in the case of SA can offer extra surface interaction possibilities than an aliphatic structure like MA. The resulting higher surface interaction may decrease the catalytic activity of the photocatalyst due to the occupation or blockage of surface reactive sites. Furthermore, the aromatic structure of SA can be responsible for light screening, in which the organic compound absorbs a portion of the light before it reaches the photocatalyst. Photocatalytic systems have also been reported to exhibit similar light-screening effects with aromatic organic compounds, along with the potential effects of radical scavenging and

competitive surface adsorption [22]. These possible mechanisms, however, were not directly evaluated in the present study. In the present work, the focus is put on the kinetic modelling and the comparison of photocatalytic performance under the different LMWOA conditions; hence the specific molecular-level mechanisms leading to the different effects of SA and MA should be mechanically investigated in future work by using dedicated surface and spectroscopic techniques. However, the kinetic results show that the carboxyl-group number and acid strength alone are not reliable indicators of an LMWOA's impact on photocatalytic kinetics, and cannot be used to predict its effect on photocatalytic treatment and energy use.

3.6 Practical Implications

The characterization, kinetic and energy-efficiency results presented here suggest that LMWOAs not only affect TC removal efficiency but have a measurable impact on the actual energy cost to achieve the photocatalytic treatment of g-C_3N_4, and to different extents depending on the type of acid. In other words, for a water utility or decentralized treatment system under variable changes in agricultural runoff or food-processing effluent composition driven by climate, this implies that the estimation of the water-matrix characterization is critical for reliable process design, with the energy penalty associated with a co-contaminant profile dominated by acids similar to MA being relatively small, and that dominated by acids similar to SA may several-fold increase the energy demands and compromise the economic and operational resilience of the treatment system [2]. The results offer an initial engineering quantitative basis for assessing the potential of g-C_3N_4 based photocatalysis under real wastewater streams with co-occurring antibiotics and organic acids, while also enabling future design of a pilot scale or a continuous flow that is in line with ENRIC 2026's focus on real-world impact and climate resilience.

4. CONCLUSIONS

This study took a deliberately modelling-oriented approach to the g-C_3N_4/TC/LMWOA system, the reaction kinetics and energy cost are what an engineer of the treatment plant needs to size and cost a real reactor, rather than to re-examine removal efficiency or reaction mechanism. Both SA and MA were chosen because they are realistic examples of TC co-contaminants and are well documented in pharmaceutical wastewater (up to 900 mg L^{-1}) and food-processing and agricultural streams (up to tens of mM), respectively, spanning the 0.5-5 mM range addressed. The pseudo-first-order model was found to be best suited in all nine conditions (R^2 = 0.969–0.993), and a single-run Langmuir–Hinshelwood analysis confirmed this, as the values of kr and K could not be resolved, with negligible *K* values and poor fit quality for the control and MA conditions, which supports PFO as the appropriate apparent kinetic description under the conditions tested, although this identifiability limitation does not by itself establish the underlying reaction mechanism. SA caused severe kinetic inhibition of 80.5–89.0% and a 4.4–7.4 fold increase in EEO, MA caused a mild inhibition of 14.4–30.5% and a 1.09–1.35 fold increase with the most energy efficient condition tested being MA at 0.5 mM. This difference did not correlate with the number of carboxyl groups or with the acidity of the carboxyl groups, suggesting the presence of other structural factors that are likely responsible, such as aromaticity and surface-binding mode. All these combined characterization, kinetic, and EEO benchmarks, based on realistic ranges of LMWOA concentration, offer scalable, decision-ready guidance for climate-resilient antibiotic-water-treatment technology based on g-C_3N_4.

Acknowledgement

This research is funded by Thailand Science Research and Innovation Fund Chulalongkorn University (DIS_FF_69_095_2100_015).

References

[1] Xu, L., Zhang, H., Xiong, P., Zhu, Q., Liao, C., & Jiang, G. (2021). Occurrence, fate, and risk assessment of typical tetracycline antibiotics in the aquatic environment: A review. *Science of The Total Environment, 753*, 141975.

[2] Madushika, N. H., Munaweera, I., Liyanage, G. Y., Jayawardane, P., & Manage, P. M. (2026). Innovative green nanotechnology for sustainable water purification under climate change: Tackling antibiotic contaminants. *Environmental Science: Nano, 13*(1), 150-183.

[3] Zhu, B., Zhang, L., Cheng, B., & Yu, J. (2018). First-principle calculation study of tri-s-triazine-based g-C3N4: A review. *Applied Catalysis B: Environmental, 224*, 983-999.

[4] Bhanderi, D., Lakhani, P., & Modi, C. K. (2023). Graphitic carbon nitride (g-C3N4) as an emerging photocatalyst for sustainable environmental applications: A comprehensive review. *RSC Sustainability, 2*(2), 265-287.

[5] Bilić, A., Armaković, S. J., & Armaković, S. (2026). Photocatalytic degradation of an aromatic pharmaceutical over TiO2: Experimental and computational insights into inhibition effects of natural organic acids. *Molecules, 31*(5), 797.

[6] Paíga, P., Figueiredo, S., Correia, M., André, M., Barbosa, R., Jorge, S., & Delerue-Matos, C. (2025). Occurrence of 97 pharmaceuticals in wastewater and receiving waters: Analytical validation and treatment influence. *Journal of Xenobiotics, 15*(3), 78.

[7] Hu, R., Zhang, L., & Hu, J. (2016). Study on the kinetics and transformation products of salicylic acid in water via ozonation. *Chemosphere, 153*, 394-404.

[8] Verdini, F., Desogus, N., Calcio Gaudino, E., & Cravotto, G. (2025). From skincare to watercare: Tackling salicylic acid pollution with hybrid glow plasma-cavitation technology. *Ultrasonics Sonochemistry, 120*, 107468.

[9] Han, Y., Su, Z., & Du, J. (2023). Effects of apple storage period on the organic acids and volatiles in apple wine. *LWT, 173*, 114389.

[10] Zhu, H., Bing, H., & Wu, Y. (2022). Citric acid promotes the mobilization of phosphorus under the lower concentration of low molecular weight organic acids in acidic forest soil. *Adsorption Science and Technology, 2022*, 5071907.

[11] Xiong, Y., Harb, M., & Hong, P. Y. (2017). Performance and microbial community variations of anaerobic digesters under increasing tetracycline concentrations. *Applied Microbiology and Biotechnology, 101*(13), 5505-5517.

[12] Yang, W., Jia, L., Wu, P., Zhai, H., He, J., Liu, C., & Jiang, W. (2021). Effect of thermal program on structure-activity relationship of g-C3N4 prepared by urea pyrolysis and its application for controllable production of g-C3N4. *Journal of Solid State Chemistry, 304*, 122545.

[13] Tran, H. D., Nguyen, D. Q., Do, P. T., & Tran, U. N. P. (2023). Kinetics of photocatalytic degradation of organic compounds: A mini-review and new approach. *RSC Advances, 13*(25), 16915-16925.

[14] Ramos-Justicia, J. F., Urbieta, A., & Fernández, P. (2026). Refined Langmuir-Hinshelwood kinetics for heterogeneous photocatalytic systems: Analytical closed-form solution, enhanced approximations and experimental validation. *PhysChem, 6*(1), 5.

[15] Keen, O., Bolton, J., Litter, M., Bircher, K., & Oppenländer, T. (2018). Standard reporting of Electrical Energy per Order (EEO) for UV/H2O2 reactors (IUPAC Technical Report). *Pure and Applied Chemistry, 90*(9), 1487-1499.

[16] Chabib, L., Nursal, Miskam, M., Kaus, N. H. M., Shafie, M. H., Hamid, M., Saragi, I. R., Isnaeni, I., Amilia, D., Dalimunthe, I. B., & Wijoyo, H. (2025). Optimization of g-C3N4 nanoparticles on structural, morphological, and optical properties as organic pollutants adsorbent in glycerin. *Case Studies in Chemical and Environmental Engineering, 11*, 101057.

[17] Kokate, S., Gupta, S., Kopuri, V. G., & Prakash, H. (2022). Energy efficient photocatalytic activation of peroxymonosulfate by g-C3N4 under 400 nm LED irradiation for degradation of Acid Orange 7. *Chemosphere, 287*, 132099.

[18] Farzadkia, M., Bazrafshan, E., Esrafili, A., Yang, J. K., & Shirzad-Siboni, M. (2015). Photocatalytic degradation of Metronidazole with illuminated TiO2 nanoparticles. *Journal of Environmental Health Science and Engineering, 13*(1), 19.

[19] Fattahi, A., Jaciw-Zurakowsky, I., Srikanthan, N., Bragg, L., Liang, R., Zhou, N., Servos, M., & Arlos, M. (2021). Effect of background water matrices on pharmaceutical and personal care product removal by UV-LED/TiO2. *Catalysts, 11*(5), 576.

[20] Li, D., Feng, Z., Zhou, B., Chen, H., & Yuan, R. (2022). Impact of water matrices on oxidation effects and mechanisms of pharmaceuticals by ultraviolet-based advanced oxidation technologies: A review. *Science of The Total Environment, 844*, 157162.

[21] Munir, S., Neal, C. J., Gillie, L. J., Cooke, D. J., Seal, S., & Molinari, M. (2025). Effect of strain on the adsorption of carboxylic acids on the surfaces of cerium oxide. *Surfaces and Interfaces, 76*, 107836.

[22] Awfa, D., Ateia, M., Fujii, M., & Yoshimura, C. (2020). Photocatalytic degradation of organic micropollutants: Inhibition mechanisms by different fractions of natural organic matter. *Water Research, 174*, 115643.